Low-Cost Automated Antenna Radiation Pattern Measurement System Based on Arduino and Raspberry Pi

Fedi MEJRI, Fethi MEJRI, Nadia FEZAI, Tijeni Delleji

***Abstract*— This paper presents the design and implementation of a low-cost, automated antenna radiation pattern measurement system based on a hybrid Arduino-Raspberry Pi architecture. The Arduino Uno provides real-time stepper motor control and RF signal acquisition, while the Raspberry Pi handles serial communication, data processing, and storage. To validate the proposed system, a circular microstrip patch antenna operating at 1.47 GHz was designed, fabricated, and experimentally characterized. The measured radiation pattern was compared to ADS simulation results, demonstrating that the proposed platform is a practical, reproducible, and affordable solution for antenna radiation pattern characterization in small research environments, with RF detector calibration over a 40 dB dynamic range confirming a mean measurement precision of ±0.71% across three independent runs.**

Keywords: antenna radiation pattern measurement, low-cost measurement system, Arduino, Raspberry Pi, RF detector, stepper motor, microstrip patch antenna.

I. INTRODUCTION

Measuring the radiation pattern of an antenna is a fundamental step in its design, performance evaluation, and electromagnetic compatibility testing. Characterizing the directional properties of an antenna requires precise angular scanning, calibrated RF detection, and accurate data acquisition—tasks traditionally performed in anechoic chambers equipped with professional antenna positioners and vector network analyzers [5], [14]. However, these facilities remain financially inaccessible to most university laboratories and small research centers, hence the significant need for cost-effective and reproducible alternatives.

Several measurement approaches have been described in the literature. High-end systems rely on calibrated RF sources, absorbing chambers, and motorized positioners, offering high accuracy but at a prohibitive cost [9]. Software-defined radio (SDR) platforms have also been explored: Perotoni et al. [6] proposed a near-field SDR system, which, however, requires complex post-processing for far-field transformation. Schottky diode RF detectors have been validated for microwave power measurement [1], [7], offering a simpler and less expensive detection alternative. On the acquisition side, Arduino platforms have demonstrated their ability to acquire real-time signals in the laboratory [3] and have been combined with MATLAB for signal processing for educational purposes [4].

Despite these contributions, many existing systems cover only part of the measurement chain (acquisition, positioning, or visualization) without integrating all functions into a single, comprehensive, and reproducible platform. Furthermore, quantitative performance indicators, such as angular resolution, measurement repeatability, and the discrepancy between simulated and measured waveforms, are often insufficiently documented.

This article presents a fully integrated, cost-effective, automated antenna radiation pattern measurement system based on a hybrid Arduino-Raspberry Pi architecture. This system combines stepper motor angular positioning, Schottky diode RF detection [1], [7], and Python-based polar visualization [3], [4]. The system is experimentally validated using a circular microstrip patch antenna operating at 1.47 GHz [14], [15]. The main contributions are: (i) the design and experimental validation of a complete, reproducible and cost-effective measurement device; (ii) a quantitative comparison between measured and simulated radiation patterns, including an analysis of the finite ground plane; and (iii) a discussion of the accuracy of angular positioning, detector calibration and measurement repeatability.

II. SYSTEM ARCHITECTURE

A. OVERALL ARCHITECTURE

The proposed measurement bench is based on a hybrid architecture combining an Arduino Uno board and a Raspberry Pi. The Arduino controls the stepper motor and performs analog acquisition of the RF detector's output signal. The Raspberry Pi handles serial communication, data logging, digital processing, and graphical visualization of the measured radiation pattern via a Python interface. This division of tasks increases the system's flexibility while maintaining a low implementation cost:

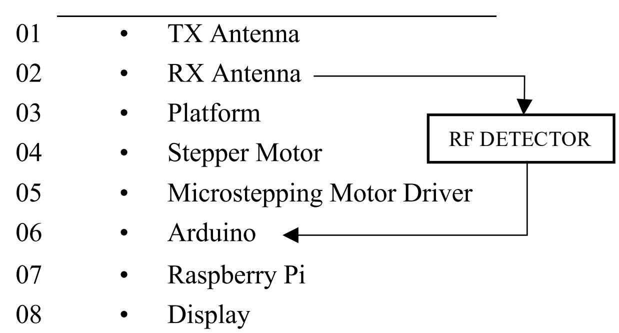

Fig. 1. Diagram Of The Radiation Pattern Measurement Setup.

Fedi Mejri, is with National Engineering School of Tunis (ENIT), Rue Béchir Salem Belkhiria Campus universitaire, BP 37, 1002, Le Bélvédère,1002,Tunis (Author's phone: +216 29563963: e-mail: fedi.mejri@etudiant-enit.utm.tn).

Fethi Mejri, is with National Engineering School of Tunis (ENIT). Rue Béchir Salem Belkhiria Campus universitaire, BP 37, 1002, Le Bélvédère, 1002, Tunis e-mail : fethi.mejri.syscom@gmail.com).

Nadia FEZAI, is with Science and Technology for Defense Lab (STD)Military Research Center, Aouina Military Base Taieb Mhiri City, 2045. Tunis, Tunisia (e-mail:nadiafezai@yahoo.fr).

Tijeni Delleji, is with Science and Technology for Defense Lab (STD)Military Research Center, Aouina Military Base Taieb Mhiri City, 2045. Tunis, Tunisia (e-mail: tijeni dalleji@yahoo.fr).

B. HARDWARE COMPONENTS

• Arduino Uno Microcontroller: The Arduino Uno is the central control unit of the system. It handles the acquisition of analog signals from the RF circuit and drives the stepper motor. The stepper motor is controlled by precise pulse sequences, ensuring accurate and consistent positioning of the mechanical structure. The output signal from the RF detector is simultaneously sampled by the integrated analog-to-digital converter (ADC), which transforms it into digital data for further processing.

• Raspberry Pi: The Raspberry Pi is the primary device for data collection and analysis. It executes Python functions for real-time analysis, visualization, and system control after receiving measurement data from the Arduino via a serial port. Thanks to its processing capabilities, it is ideally suited for coordinating multiple components within a compact measurement platform, enabling efficient handling of large volumes of data and signal processing tasks.

• External Microstepping Motor Driver: By dividing each full step into many microsteps, the external microstepping controller provides precise control of the stepper motor. Compared to full-step operation, this method produces smoother motion, better angular resolution, and reduced mechanical vibration. The Arduino sends STEP and DIR signals to the controller, enabling the precise motor movements necessary for accurate antenna positioning.[2] A 1/16 microstepping mode (3200 steps per rotation) was achieved by setting switches SW1, SW2, and SW3 to OFF, OFF, and ON, respectively. For antenna radiation pattern measurements, this configuration offers a good compromise between rotational smoothness and angular resolution. A rated current of approximately 1.5 A was achieved by adjusting the switches SW4, SW5, and SW6 (OFF, ON, OFF). [13]

• Stepper Motor: The SM24240 stepper motor was chosen due to its high torque and precise positioning, which are essential for measurement applications. Even at low rotational speeds, its torque capabilities enables it to carry relatively large loads, like an antenna mounted on a spinning structure, without losing steps.

• RF detector: The received RF signal is converted to a DC voltage using a diode-based RF detector, illustrated in Figures 3 and 4. This detector consists of two BAT68 Schottky diodes and a 100 nF filter capacitor. Schottky diodes are used because of their low forward voltage and low junction capacitance, making them particularly suitable for detecting RF signals. The detector's output voltage is applied to the Arduino's analog input. Although absolute power calibration is not required for relative radiation pattern measurements, a calibration procedure was performed to characterize the detector response and quantify its measurement repeatability, as described below.

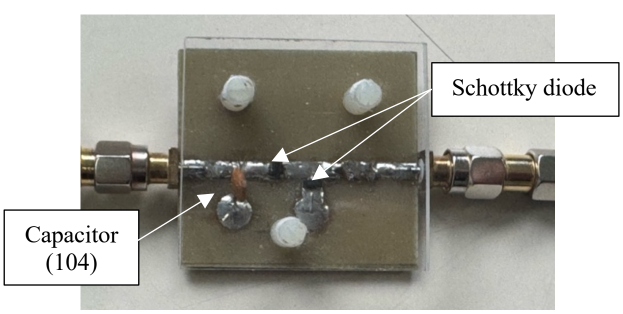

Fig. 2. Diode-Based RF Detector Used for Power Measurement

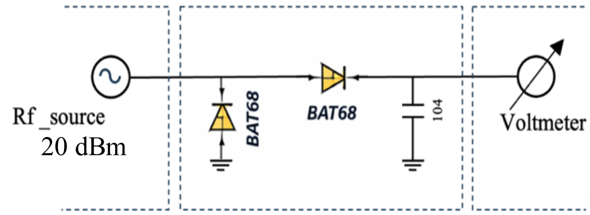

Fig. 3. Schematic Diagram Of The Dual Schottky Diode RF detector

RF detector calibration : To characterize the response of the BAT68 Schottky diode RF detector, a calibration procedure was performed by applying known RF power levels at the operating frequency of 1.47 GHz using a calibrated signal generator. The DC output voltage was recorded for input power levels ranging from −30 dBm to +10 dBm in 1 dBm increments. The resulting calibration curve, shown in Figure 4, exhibits a monotonically increasing response over the entire 40 dB dynamic range. In the low-power range (−30 to −8 dBm), the detector operates in quadratic mode, where the output voltage is approximately proportional to the incident RF power. Beyond −8 dBm, the slope of the response increases, indicating a transition to the linear detection regime, consistent with the behavior observed for similar Schottky detectors [7], [9].

Since the proposed system is designed for relative measurement of the radiation pattern, the detected voltage is normalized with respect to its maximum value before the polar diagram is reconstructed. This normalization eliminates the absolute gain offset and preserves the angular dependence of the radiation pattern regardless of the detector's operating region, as expressed in section IV by $V\_out(\theta) \propto |E(\theta)|^{2n}$, where the exponent n depends on the operating region and is determined experimentally from the calibration curve. [9].

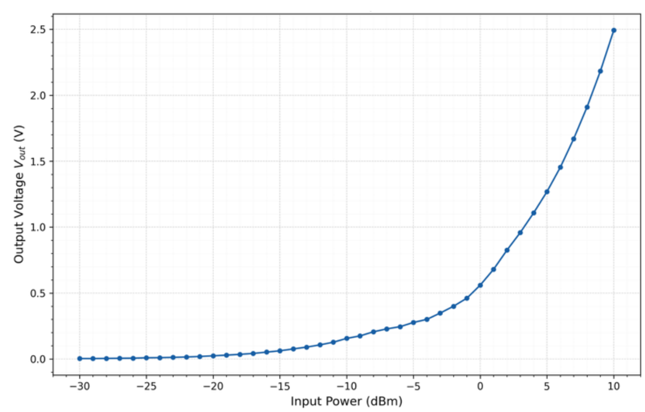

Fig. 4. Calibration Curve Of The RF Detector At 1.47 Ghz

To evaluate the repeatability of the detector response, three independent measurement runs were performed under identical conditions. The measurement precision, defined as the standard deviation normalized to the mean reading at each power level, is shown in Fig. 5. The mean precision across the entire dynamic range was ±0.71% of the reading, with a maximum of ±4.04% observed around −1 dBm, in the transition zone between the square-law and linear detection regimes. Over the operating range of interest for antenna pattern measurement (−20 to −8 dBm), the precision remained below ±2.7%, confirming the consistency and suitability of the RF detection chain for relative radiation pattern characterization.

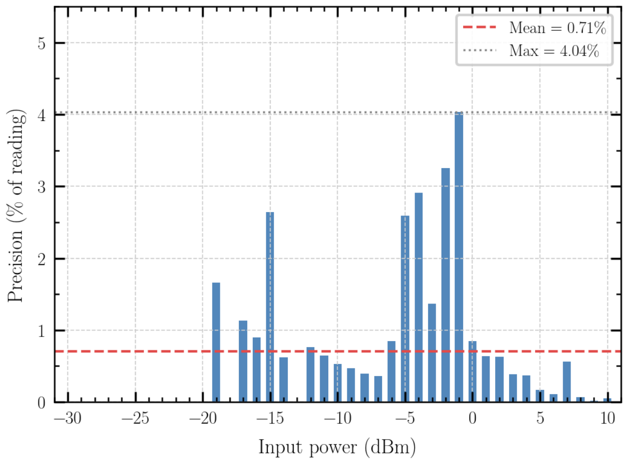

Fig. 5. Measurement Precision Of The RF Detector

• Mechanical Rotating Platform: To provide mechanical stability and consistent angular alignment during measurements, the antenna under test (AUT) is mounted on a rotating platform.

• Receiving Antenna Support: To reduce electromagnetic interference during the measurement procedure, the receiving antenna is fixed on a non-conductive mechanical arm.The distance between the two antennas is selected according to the far-field condition discussed in Section II-E.

C. Power Supply and Electrical Connections:

Element	**Supply Voltage**
Microstep Driver	09–42 V
Arduino	5 V
Raspberry Pi	5 V

TABLE1: Power Supply Voltages Of The System Components.

Microstep Driver	**Arduino**
PUL+ (STEP+)	Pin 8
PUL−	GND
DIR+	Pin 3
DIR−	GND
ENA+	Pin 5
ENA −	GND
RF detector	**Arduino**
V_out	**A0**
GND	GND

TABLE 2 : Electrical Connections Between Arduino, Microstepping Driver, and RF detector.

The practical wiring of the measurement bench is shown in Fig. 5. The Arduino generates the STEP, DIR, and ENABLE control signals for the microstepping driver, while the RF detector output is connected to analog input A0. The Arduino and Raspberry Pi communicate through a USB serial connection.

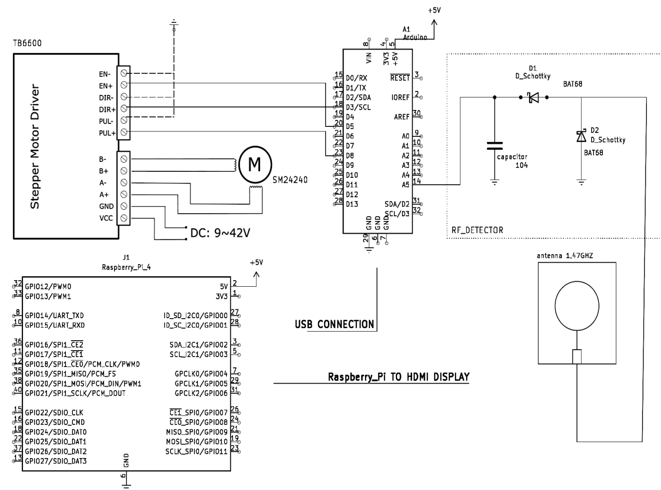

Fig. 6. Electrical Setup Of The Antenna Radiation Pattern Measurement System

D. SOFTWARE ARCHITECTURE:

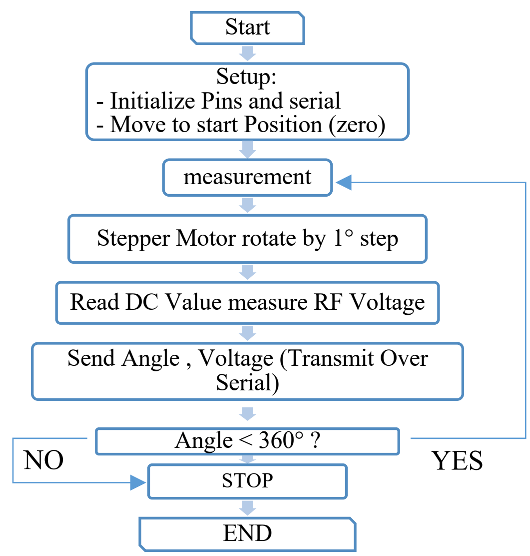

Fig. 7. Arduino Firmware Flowchart.

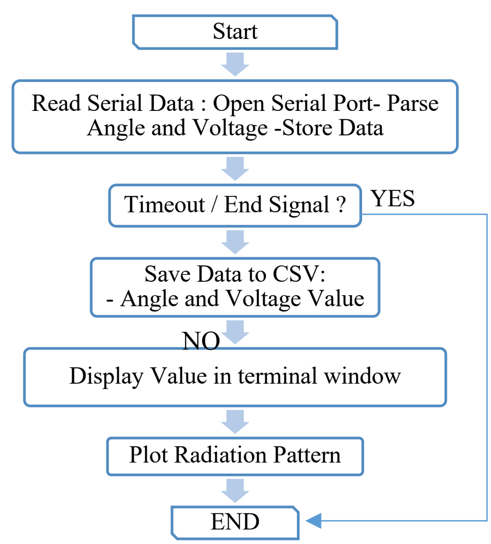

Fig. 8. Python Software Flowchart

The measured angle and voltage values sent by the Arduino are read in real-time using a Python program. The data are stored in a CSV file for easy analysis and traceability. Python libraries are then used to organize the measurements and generate a polar plot, allowing a clear and intuitive visualization of the antenna radiation pattern. [3], [4].

E. SPATIAL ARRANGEMENT:

In order to ensure that the radiation pattern was measured under far-field conditions, the distance between the transmitting antenna and the antenna under test was selected such that :

$$R \geq \frac{2D^2}{\lambda} \qquad (1)$$

Where D is the maximum antenna dimension and λ is the wavelength at the operating frequency. During the experiments, the separation distance was chosen to satisfy this criterion while remaining compatible with the laboratory constraints. [5], [14]

In addition to the far-field condition, classical antenna measurement relations such as the Friis transmission equation (2), free-space path loss (3), and angular resolution formulas were used to justify the experimental setup and measurement accuracy.

Friis Transmission Equation:

$$P_r = P_t + G_t + G_r - L_{fs} \qquad (2)$$

- Pt = transmitted power
- Pr = received power
- Gt,Gr = antenna gains
- Lfs = free-space loss

Free-Space Path Loss (FSPL):

$$L_{fs}(dB) = 20\, log_{10}(\frac{4\pi R}{\lambda}) \qquad (3)$$

III. ANTENNA DESIGN AND ADS SIMULATION

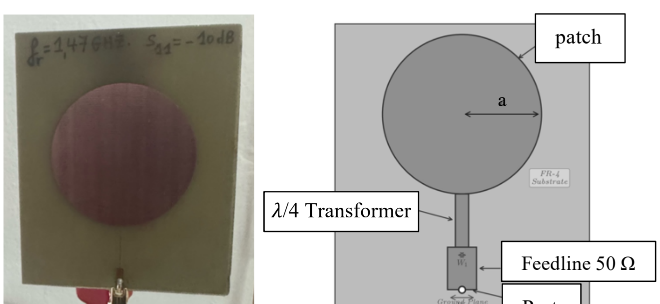

Fig. 9. Antenna Under Test (AUT)

A. Substrate and Material Selection

The antenna is designed on a FR-4 substrate due to its low cost and widespread availability in PCB technology. The substrate parameters are as follows: [15], [10]

- Relative permittivity: ε_r= 4.32
- copper conductivity : σ =59.6 . 10^6 S/m
- Relative permeability: μr=1
- Substrate thickness: h=1.5 mm
- Copper thickness: t=35 μm
- Conductor material: Copper
- Substrate material in ADS: FR_4_Core

B. Patch Antenna Design

For a circular microstrip patch antenna operating in the dominant TM_{11} mode, the resonant frequency can be approximated by:

$$f_r = \frac{X_{11}\ c}{2\,\pi\, a\,\sqrt{\varepsilon_r}} \qquad (4)$$

Where a is the patch radius, c is the speed of light, ε_r is the relative permittivity of the substrate, and X_{11} =1.8412 is the first root associated with the dominant TM_{11} mode. [14] Therefore, the initial patch radius is obtained from:

$$a = \frac{X_{11}\ c}{2\,\pi\, f_r\,\sqrt{\varepsilon_r}} \qquad (5)$$

After calculation based on equation (4) and tuning in ADS, the optimized patch radius is: a = 28.899 mm

C. Quarter-Wave transformer

A narrow microstrip line is connected directly to the circular patch :

- Width: W1=1.023 mm
- Length: L1=29.427 mm (λ/4 at 1.47 GHz)

D. Feedline

The 50 Ω microstrip line connects the λ/4 matching section to the measurement port:

- Width: W2 = 2.874 mm
- Length: L2 = 10 mm

This section provides a standard 50 Ω connection for the test equipment. All dimensions are calculated using **ADS LineCalc** [15] , where we input:

- Desired characteristic impedance Z0 = 50 Ω
- Effective electrical length θ = 90° (λ /4)
- Substrate parameters (mentioned before)

ADS automatically computes the line width and length to satisfy the impedance transformation.

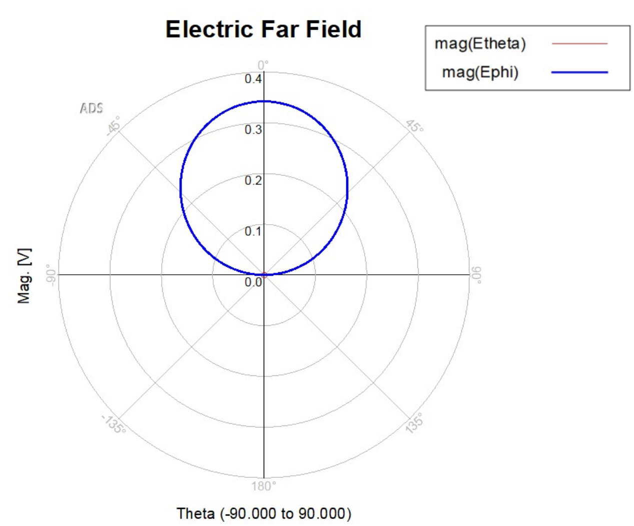

Fig. 10. Simulated Radiation Pattern of the Circular Patch Antenna at 1.47 GHz

IV. EXPERIMENTAL RESULTS

The proposed antenna radiation pattern measurement setup was validated through experimental measurements after the mechanical design and system assembly were finalized. With the transmitting antenna positioned at a distance meeting the far-field criterion, the antenna under test was mounted on the rotating platform. A stepper motor rotated the antenna in discrete angular increments during the measurement.

The RF signal captured by the RF detector was applied to an analog input of the Arduino, which transmitted the measured data to a computer via a serial interface. At each assembly stage, basic functional tests were performed to verify the proper operation of the motor, sensors, and serial communication before launching the automated measurement sequences.

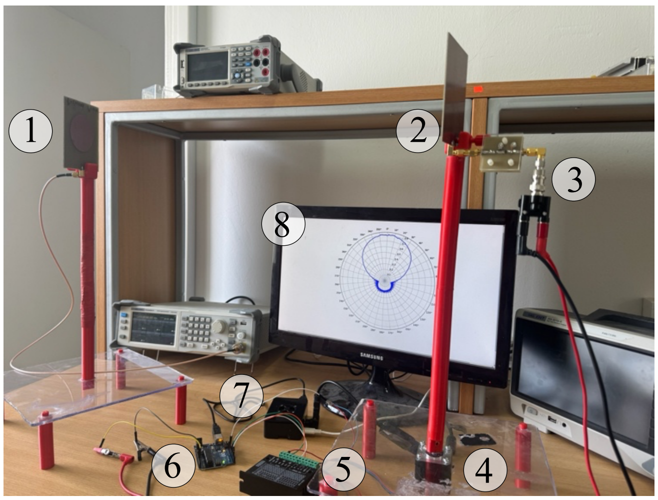

Fig. 11. Experimental setup for antenna radiation pattern measurement

1- TX Antenna
2- RX Antenna
3- RF detector
4- Stepper Motor
5- Microstepping Motor Driver
6- Arduino
7- Raspberry Pi
8- Display

In the far-field region, the power received by an antenna is proportional to the square of the incident electric field magnitude [5], [9] :

$$P_{RF}(\theta) \propto |E(\theta)|^{2} \qquad (6)$$

- PRF(θ) is the received RF power
- E(θ) is the electric field strength at angle

For the diode RF detector, the output voltage is :

$$V_{out} \propto P_{RF}^{n} \qquad (7)$$

- V_out is the detected DC voltage
- n is a coefficient depending on the operating region of the diode.

Then, by combining the two previous formulas, we can define the expression that preserves the angular dependence :

$$V_{out}(\theta) \propto |E(\theta)|^{2n} \qquad (8)$$

This nonlinearity affects the absolute amplitude but preserves the angular dependence of the received signal, which is sufficient for characterizing the radiation pattern [5], [14]. By normalizing the detected voltage to its maximum value and expressing it in decibels, the antenna's radiation pattern can be accurately reconstructed as a function of angular position.

The measured data were transmitted via the serial interface to a processing unit, where they were stored and visualized using a Python data acquisition and visualization script. The resulting polar radiation pattern clearly reveals the antenna's directional characteristics, including the main lobe orientation, beamwidth, and relative levels of the sidelobes. The smooth angular variation of the measured signal confirms the mechanical stability of the rotating platform and the effectiveness of the microstepping motor control.

V. RESULTS ANALYSIS

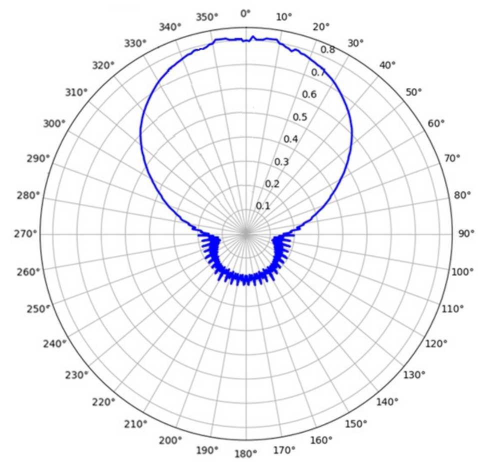

Fig. 12. Measured Radiation Pattern of the Circular Patch Antenna at 1.47 GHz.

To evaluate the quantitative performance of the proposed measurement system, several parameters were considered, including angular resolution, measurement step size, repeatability, and the difference between simulated and measured radiation patterns. The external microstepping driver was configured in 1/16 microstepping mode, corresponding to 3200 microsteps per complete revolution. The theoretical angular resolution of the rotating platform is therefore given by:

$$\Delta\theta = \frac{360°}{3200} = 0.1125° \qquad (9)$$

Although the motor can provide a theoretical resolution of 0.1125°, the experimental radiation pattern was acquired with an angular step of 1°. This value was chosen as a compromise between measurement time, data size, and angular accuracy. Thus, 360 measurement points were recorded over one complete rotation.

The RF detector used in this work is based on Schottky diodes. Although this solution is simple and economical, the detector output voltage is not perfectly linear with the incident RF power. In the square-law region, the detected voltage is approximately proportional to the received RF power, whereas nonlinear effects outside this region may introduce amplitude deviations, particularly in sidelobe measurements.

The calibration results presented in Section II-B confirm that the detector operates within the square-law region for the received power levels encountered during antenna pattern measurement, validating the normalization approach adopted in this work. Therefore, the measured voltages were normalized to their maximum value to reconstruct the relative radiation pattern:

$$V_{norm}(\theta) = \frac{V_{out}(\theta)}{V_{out,max}(\theta)} \quad (10)$$

For absolute power measurements, a calibration procedure is required. This can be performed by applying known RF power levels at the operating frequency of 1.47 GHz using a calibrated RF source or signal generator. For each input power level, the corresponding DC output voltage of the detector is recorded. In this work, the objective is to characterize the relative radiation pattern; therefore, normalization was deemed sufficient to identify the main radiation behavior of the antenna.

The measurements were performed in a non-anechoic laboratory environment. Consequently, the measured radiation pattern can be affected by reflections from surrounding objects, walls, cables, the support structure, and the measurement table. These multipath effects can produce constructive and destructive interference, resulting in local amplitude variations and sidelobes in the measured pattern. In addition, mechanical tolerances of the rotating platform, slight antenna misalignment, finite ground plane effects, and RF detector nonlinearity may contribute to the observed differences between simulated and measured results.

Parameter	Method /Expression	Value
Microstepping mode	Driver configuration	1/16
Microsteps per revolution	Motor driver setting	3200
Theoretical angular resolution	360° / 3200	0.1125°
Experimental angular step	Software-defined rotation step	1°
Number of angular samples	360° / 1°	360
Main-lobe direction error	|θ_meas − θ_sim|	2°
Repeatability error	Standard deviation over 3 repeated scans	±0.7°

TABLE 3 : Quantitative Performance Metrics of the Proposed Measurement System

A significant difference is observed between the simulated and measured radiation patterns. The ADS simulation assumes idealized boundary conditions, while the fabricated antenna operates with a finite-dimensional ground plane and in a real measurement environment. Consequently, edge diffraction and surface current reflections at substrate interfaces can generate additional radiation components that are not fully accounted for by the ideal simulation. Despite these differences, the measured pattern retains the expected behavior of the main lobe of the patch antenna.

VI. CONCLUSION

This paper presents the design and implementation of a low-cost, automated antenna radiation pattern measurement system based on a hybrid Arduino-Raspberry Pi architecture. The proposed device combines motorized angular positioning, RF detector acquisition, and data visualization via Python, all on a compact and affordable platform suitable for educational applications and small laboratories.

The system was experimentally validated using a circular microstrip patch antenna operating at 1.47 GHz, and the measured radiation pattern was compared to ADS simulation results. This comparison demonstrated that the proposed test bench is capable of reproducing the main characteristics of the antenna radiation pattern, while also revealing the influence of practical factors such as detector nonlinearity, the finite size of the ground plane, and environmental reflections.

Future work will focus on improving detector calibration, extending quantitative assessment, reducing environmental effects, and upgrading the platform to measure two-dimensional or three-dimensional radiation patterns.

VII. ACKNOWLEDGMENT

This research was conducted with the support and funding of the National Engineering School of Tunis (ENIT), the University of Tunis El Manar, and the Military Research Center (MRC), Tunis, Tunisia. The authors express their sincere gratitude to **Dr. Eng. Ahmed Siala**, General Director of the Military Research Center, for his valuable assistance, and for providing the necessary resources that contributed significantly to the successful achievement of this work.

VIII. REFERENCES

[1] Ali, M., Ibrahim, S., Adam, I., & Khalid, N. (2019). Design and development of RF power detector for microwave application. Indonesian Journal of Electrical Engineering and Computer Science. https://doi.org/10.11591/ijeecs.v13.i2.pp713-720.

[2] The characteristics of TB6600 motor driver in producing optimal movement for the Nema23 stepper motor on CNC machine (2020). http://doi.org/10.12928/telkomnika.v18i1.12781

[3] D'Ausilio, A. (2011). Arduino: A low-cost multipurpose lab equipment. Behavior Research Methods, 44, 305 - 313. https://doi.org/10.3758/s13428-011-0163-z.

[4] Arreguin-Juárez, M., Hernández-López, S., Sánchez-Torrecitas, E., & Quintanilla-Domínguez, J. (2020). System of acquisition and processing of signals through of Arduino platform and Matlab (How tool of learning). , 19-27. https://doi.org/10.35429/jti.2020.20.7.19.27.

[5] IEEE standard test procedures for antennas, ANSI/IEEE Std 149-1979 (1979) 1–144, http://dx.doi.org/10.1109/IEEESTD.1979.120310.

[6] M.B. Perotoni, L.A. da Silva, W.J. Silva, K.M.G. Santos, Near-field measurement system based on a software defined radio, Prog. Electromagn. Res. Lett. 102 (2022) 87–94, http://dx.doi.org/10.2528/pierl21111106.

[7] Zhang, H., Hu, J., Li, L., Xin, J., & Wang, D. (2019). Design of LTE-Band Microwave Power Detection System Based on Schottky Diode. IEEE Sensors Journal, 19, 3425-3430. https://doi.org/10.1109/jsen.2019.2893732.

[8] J. R. James and P. S. Hall, *Handbook of Microstrip Antennas*, London, U.K.: Peter Peregrinus Ltd., 1989.

[9] D. M. Pozar,*Microwave Engineering*, 4th ed., Hoboken, NJ, USA: John Wiley & Sons, 2012.

[10] R. Garg et al.**,** *Microstrip Antenna Design Handbook*, Artech House, 2001.

[11] Al-Amoudi, M. (2021). STUDY, DESIGN, AND SIMULATION FOR MICROSTRIP PATCH ANTENNA. International Journal of Applied Science and Engineering Review.

[12] Merino-Fernandez, I., Del Pino, J., & Khemchandani, S. (2025). Design of rectangular patch antennas through machine learning. Scientific Reports, 15. https://doi.org/10.1038/s41598-025-18939-2.

[13] "HARDWARE DRIVER MOTEUR PAS A PAS," RedOhm, published 29 April 2016. [Online]. Available: https://www.redohm.fr/2016/04/hardward-driver-moteur-pas-a-pas/

[14] C. A. Balanis, *Antenna Theory: Analysis and Design*, 4th ed. Hoboken, NJ, USA: Wiley, 2016.

[15] K. F. Lee and K. M. Luk, "Microstrip Patch Antennas," Imperial College Press, London, 2011